# Magnetic and Optical Properties of Transition Metal (Cr, Mn, Fe, Co, and Ni) Doped Lead-Free Ferroelectric $Bi_{0.5}Na_{0.5}TiO_3$ Materials

Dang Duc Dung[1(✉)], Nguyen Hoang Thoan[1], Nguyen Huu Lam[1], Vu Tien Lam[1], Nguyen Ngoc Trung[1], Nguyen Hoang Linh[1], and Duong Quoc Van[2]

[1] Multifunctional Ferroics Materials Lab, School of Engineering Physics, Ha Noi University of Science and Technology, 1 Dai Co Viet Road, Hanoi, Viet Nam
dung.dangduc@hust.edu.vn

[2] Faculty of Physics, Ha Noi National University of Education, 136 Xuan Thuy Road, Hanoi, Viet Nam
vandq@hnue.edu.vn

**Abstract.** In this work, transition metals, including Cr, Mn, Fe, Co, and Ni, were selected as doping impurities in host lead-free ferroelectric $Bi_{0.5}Na_{0.5}TiO_3$ materials. The X-ray diffraction study revealed that transition-metal cations were incorporated into the $Bi_{0.5}Na_{0.5}TiO_3$ host crystals, resulting in lattice distortion. Complex magnetic properties of transition metal-doped lead-free ferroelectric $Bi_{0.5}Na_{0.5}TiO_3$ materials were obtained. The optical bandgap of the pure $Bi_{0.5}Na_{0.5}TiO_3$ material was estimated at around 3.09 eV, which was decreased to 2.69 eV, 2.03 eV, 2.71 eV, 2.23 eV, and 2.88 eV for Cr-, Mn-, Fe-, Co-, and Ni-dopants random incorporated into the $Bi_{0.5}Na_{0.5}TiO_3$ host crystals, respectively. The first principle theoretical calculations were performed to investigate the influence of transition metal cations substituted into the host $Bi_{0.5}Na_{0.5}TiO_3$ materials. We expected that our work could further explain the role of transition metals on the properties of lead-free ferroelectric materials.

**Keywords:** $Bi_{0.5}Na_{0.5}TiO_3$ · Lead-free ferroelectric · Ferromagnetic · Sol-gel

## 1 Introduction

Recently, advanced functional ferroelectric materials are new electronic materials that could make the next generation of smart electronic devices [1]. The toxic lead-based ferroelectric $Pb(Zr,Ti)O_3$-based materials are currently used worldwide in electric devices because of their excellent properties [2]. Therefore, looking for green ferroelectric materials to replace lead-based ferroelectric materials in electronic devices is needed. Among lead-free ferroelectric materials, bismuth sodium titanate ($Bi_{0.5}Na_{0.5}TiO_3$) materials were candidates for replacing lead-based ferroelectric materials because the materials had large remnant polarization of about 38 $\mu C/cm^2$ and Curie temperature of about 320 °C, respectively [3].


B. T. Long et al. (Eds.): AMAS 2021, LNME, pp. 610–614, 2022.
https://doi.org/10.1007/978-3-030-99666-6_88

Recently, the observation of weak-ferromagnetic properties of lead-free ferroelectric $Bi_{0.5}Na_{0.5}TiO_3$ materials was promised to create a new type of electronic devices that uses both ferromagnetic and ferroelectric properties [4, 5]. In fact, various transition metals were incorporated with the $Bi_{0.5}Na_{0.5}TiO_3$ host lattices to enhance the magnetic moment and reduce the optical bandgap of host materials such as Cr, Mn, Fe, Co, and Ni [4, 5]. However, so far, the previous studies did not mention the origin of reduction in the bandgap of transition-metal doped-BNT materials.

In this work, the lead-free ferroelectric $Bi_{0.5}Na_{0.5}Ti_{0.97}Tr_{0.03}O_3$ ($Tr$ = Cr, Mn, Fe, Co, Ni) materials were synthesized using the sol-gel technique. The complex magnetic properties were obtained, dependent on the doping type. The optical bandgap was reduced after incorporating transition-metal cations into the host lattices. The influence of transition metals on the electric band structure of $Bi_{0.5}Na_{0.5}TiO_3$ materials was studied using the first principle theoretical calculations.

## 2 Experimental

Pure $Bi_{0.5}Na_{0.5}TiO_3$ and $Bi_{0.5}Na_{0.5}Ti_{0.97}Tr_{0.03}O_3$ materials ($Tr$ = Cr, Mn, Fe, Co and Ni) (named as BNT, and BNT-Cr, BNT-Mn, BNT-Fe, BNT-Co, and BNT-Ni, respectively), were well synthesized by a chemical method. Raw materials included $Bi(NO_3)_3.5H_2O$, $NaNO_3$, $C_{12}H_{28}O_4Ti$, $Cr(NO_3)_3.9H_2O$, $Mn(NO_3)_2$ solution, $Fe(NO_3)_3.9H_2O$, $Co(NO_3)_3.6H_2O$, and $Ni(NO_3)_3.6H_2O$. Buffer solutions were aqueous acetic acid solutions with de-ion-water were used to dissolve $Bi(NO_3)_3.5H_2O$ and $NaNO_3$. Subsequently, a selected transition metal salt, including $Cr(NO_3)_3.9H_2O$, $Mn(NO_3)_2$ solution, $Fe(NO_3)_3.9H_2O$, $Co(NO_3)_3.6H_2O$, or $Ni(NO_3)_3.6H_2O$, was added. Thus, acetylacetone was dropped into the solution before dropping $C_{12}H_{28}O_4Ti$. The dry gels were annealed in air at 900 °C for 5 h. The detailed fabrication processes are summarized in Fig. 1. The chemical composition of as-prepared samples was qualified by energy dispersion X-ray spectroscopy (EDX). The crystal structure, the optical properties were studied by the X-ray diffraction technique (XRD) and Ultraviolet-Visible spectroscopy (UV-Vis) methods. The magnetic hysteresis loops were recorded by a vibrating sample magnetometer (VSM). All *ab*-initio calculations for transition metal-doped at Ti-site of BNT materials were performed using the CASTEP module in the Materials Studio software.

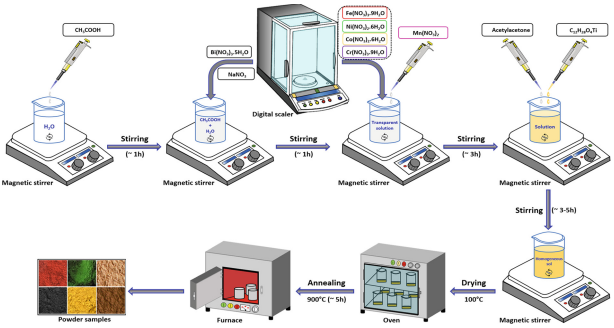


**Fig. 1.** Fabrication processes for the pure $Bi_{0.5}Na_{0.5}TiO_3$ and $(Bi_{0.5}Na_{0.5})_{0.97}Ti_{0.97}Tr_{0.03}O_3$ samples.

## 3 Results and Discussion

The EDX spectra of pure BNT and transition metal (Cr, Mn, Fe, Co, and Ni)-modified BNT materials were shown in Fig. 2(a)–(f), respectively, indicating the presence of all expected elements in the as-prepared samples.

Figure 3(a) showed the XRD spectra of the BNT and transition-metal-doped BNT samples in the 2θ-range of 20°–70°. The crystal structure of their sample was indexed as rhombohedral symmetry without the observation of impurities phases [4, 5]. The role of transition metals randomly incorporated into the host lattice BNT was studied by magnifying XRD spectra in the 2θ-range of 31.5°−33.5° for (012)/(110) couple peaks, as shown in Fig. 3(b), where the (012)/(110) couple peaks shown the complex distortion, resulting from the random distribution of Cr, Mn, Fe, Co, Ni impurity cations and the size Ti of host cations with different sizes [6]. The observation in distortion of the host BNT crystals as a function of transition-metal types was solid evidence for incorporating impurities into the host crystals.

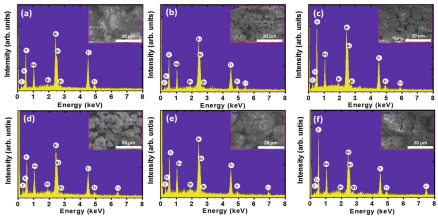


**Fig. 2.** EDX spectra of (a) BNT, and transition-metal-doped BNT materials with (b) Cr, (c) Mn, (d) Fe, (e) Co, and (f) Ni. The inset of each figure showed a selected area to determine chemical compositions.

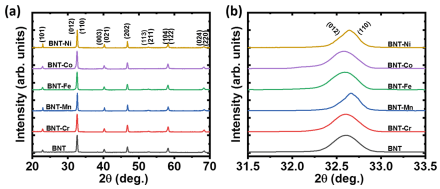


**Fig. 3.** (a) XRD spectra of the pure BNT and transition-metal-doped BNT samples in 2θ range from 20°–70°, and (b) magnification of 2θ range from 31.5°–33.5° for (012)/(110) couple peaks.

The magnetic hysteresis (M-H) loops at room temperature in Fig. 4(a) showed the influence of transition metals on the magnetic properties of the host BNT materials. The anti-*S*-shape M-H curve of the pure BNT material was related to the compensation of weak-ferromagnetic and diamagnetic properties [5]. The anti-S-shape was changed to an S-shape in the case of Fe- and Mn-doping, while it still remained in the case of Cr-, Co- and Ni-doping, indicating that the magnetic properties of transition metal-doped BNT materials were enhanced but strong depended on the type of transition metal dopants.

Figure 4(b) showed the UV-Vis spectra of pure BNT and transition metal doped BNT materials. A single band with an edge around 420 nm and the tails of the absorption spectra prolonged to 600 nm were obtained in pure BNT materials [5]. A shoulder beside the absorption edge was observed for the cases of Cr- and Fe-doping, while the hump was tailored in absorption spectra in the cases of Mn-, Co-, and Ni-dopants. In addition, the absorption edges of BNT host materials shifted to higher wavelengths, indicating a reduction of the optical bandgap values.

The optical bandgap ($E_g$) of the pure BNT and transition metal-modified BNT materials were estimated by the Wood-Tauc method [5]. Figures 5(a)–(f) showed the plots $(\alpha h\gamma)^2$ vs. $(h\gamma)$ for the pure BNT and Cr-, Mn-, Fe-, Co-, and Ni-doped BNT materials,

respectively. The $E_g$ value of the pure BNT was estimated at around 3.09 eV, which was reduced to 2.69 eV, 2.03 eV, 2.71 eV, 2.23 eV, and 2.88 eV for the samples doped with 3 mol.% Cr, Mn, Fe, Co, or Ni, respectively. The comparison of the $E_g$ values as a function of doping types was presented in Fig. 5(g). The reduction of $E_g$ values of BNT materials was less effective in the case of Cr, Fe, and Ni impurities incorporated in the BNT host lattice.

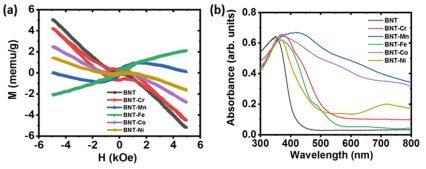


**Fig. 4.** (a) M-H curves and (b) UV-Vis spectra of the pure BNT and 3 mol.%. Cr-, Mn-, Fe-, Co-, and Ni-doped BNT materials.

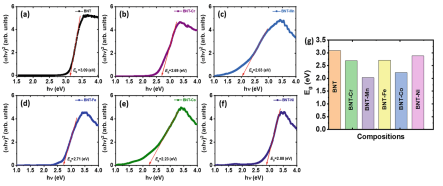


**Fig. 5.** The plots of $(\alpha h\gamma)^2$ vs. $(h\gamma)$ for (a) the pure BNT and doped BNT materials with 3 mol.% of (b) Cr, (c) Mn, (d) Fe, (f) Co, and (g) the dependence of bandgap on transition-metal doping type.

Figure 6 showed the electronic band structure, the total density of state (DOS), and the partial densities of state (PDOS) of each element in BNT. The Fermi level ($E_F$) was set to zero. The electronic band structure of BNT materials exhibited a direct transition from the top of the valence band (VB) to the bottom conduction band (CB). The $E_g$ was estimated at around 2.87 eV, relating to the transitions from O-2*p* to Ti-3*d* levels. The PDOS exhibited that the CB mainly was constructed from Ti-3*d* and Bi-6*p* while the VB was built up from O-2*p* and Bi-6*s*. The contribution of Ti-3*d* and Bi-6*s* to the VB and O-2*p* to the CB was negligible.

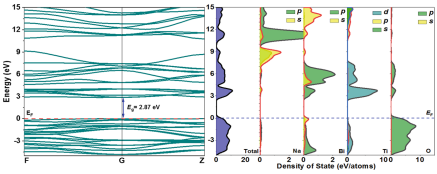


**Fig. 6.** Electronic band structure, DOS, and PDOS of BNT materials.

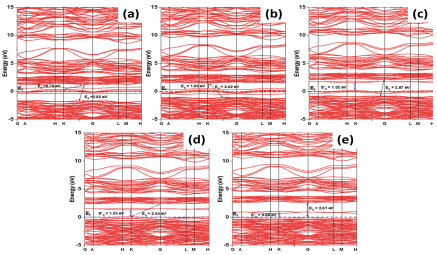


**Fig. 7.** Electronic band structures of BNT materials doped with (a) Cr, (b) Mn, (c) Fe, (d) Co, and (e) Ni impurities.

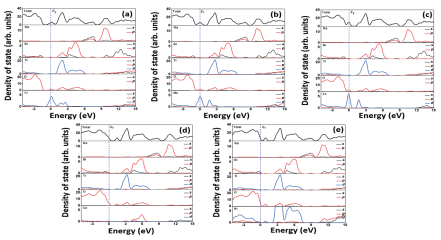


**Fig. 8.** DOS and PDOS of BNT materials doped with (a) Cr, (b) Mn, (c) Fe, (d) Co, and (e) Ni impurities.

Figures 7(a)–(e) showed the electronic band structures of BNT doped with Cr, Mn, Fe, Co, and Ni, respectively. The results exhibited that transition-metal local electronic

band structures were stable in the middle bandgap of the BNT host materials. The Fermi level is laid on the VB top in the case of Co- or Ni-doped BNT, while the Fermi is located at the local energy bands of Cr, Mn, and Fe doped at the octahedral site of BNT. The main gaps were estimated at around 2.82 eV, 2.42 eV, 2.87 eV, 2.34 eV, and 2.61 eV for the BNT crystal doped with Cr, Mn, Fe, Co, and Ni at Ti-site, respectively. In addition, the local energy levels were split under the crystal field of BNT, leading to various possible transitions.

Figures 8(a)–(e) showed the DOS and PDOS of transition metal-doped BNT materials with Cr, Mn, Fe, Co, and Ni doping, respectively. The DOS results exhibited that $E_F$ level located at the middle of the bandgap for Cr-, Mn- and Fe-doped BNT materials while the $E_F$ levels laid down on the top of VB as shown in Fig. 8(a)–(e), respectively. The PDOS results exhibited that 3*d* orbitals of Cr, Mn, Fe, and Ni were strong hybrid with the CB and VB while less obtained in Co impurities. The complex PDOS of transition metal under crystal field of lead-free ferroelectric BNT materials resulted in complex observation in absorption spectroscopy.

## 4 Conclusion

Transition metal-doped lead-free ferroelectric $Bi_{0.5}Na_{0.5}TiO_3$ materials were systematically synthesized by the chemical method. The random distribution of transition metals in the host $Bi_{0.5}Na_{0.5}TiO_3$ lattices led to the complex magnetic properties and the optical-bandgap reduction. The first principle density functional theory calculations provided that the 3*d* level of transition metals were strongly split under the crystal field of $Bi_{0.5}Na_{0.5}TiO_3$ materials. We expected that our work could further contribute to selecting impurities in lead-free ferroelectric materials.

**Acknowledgment.** We would like to acknowledge the financial support from Vietnam National Foundation for Science and Technology Development (NAFOSTED) under grant number 103.02-2019.366. This work was partially supported by The Ministry of Science and Technology, Viet Nam, under project number ĐTĐLCN.29/18.

## References

1. Mikolajick, T., et al.: Next generation ferroelectric materials for semiconductor process integration and their applications. J. Appl. Phys. **129**, 100901 (2021)
2. Smolensky, G.A., Isupov, V.A., Agranovskaya, A.I., Krainic, N.N.: New ferroelectrics with complex compounds. Fizika Tverdogo Tela **2**, 2982–2985 (1960)
3. Quan, N.D., Bac, L.H., Van Thiet, D., Hung, V.N., Dung, D.D.: Current development in lead-free $Bi_{0.5}(Na,K)_{0.5}TiO_3$-based piezoelectric materials. Adv. Mater. Sci. Eng. **2014**, 1–13 (2014)
4. Lin, J., Shi, C., Sun, L., Zhang, Y., Qin, H., Jifan, H.: Room-temperature magnetoelectric coupling in nanocrystalline $Na_{0.5}$ $Bi_{0.5}$ $TiO_3$. J. Appl. Phys. **116**(8), 083909 (2014)
5. Hung, N.T., et al.: Intrinsic and tunable ferromagnetism in $Bi_{0.5}Na_{0.5}TiO_3$ through $CaFeO_{3-\delta}$ modification. Sci. Rep. **10**(1), 6189 (2020)
6. Shannon, R.D.: Revised effective ionic radii and systematic studies of interatomic distances in halides and chalcogenides. Acta Crystallographica A **32**, 751–767 (1976)